DMD Fast Forward. Published on March 19, 2007 as doi:10.1124/dmd.106.014290

DMD #14290

Metabolism and Pharmacokinetics of a Novel Src Kinase Inhibitor TG100435 and its Active *N*-oxide Metabolite TG100855

Steven X. Hu, Richard Soll, Shiyin Yee, Daniel L. Lohse, Ahmed Kousba, Binqi Zeng, Xiyun Yu, Andrew McPherson, Joel Renick, Jianguo Cao, Arek Tabak, John Hood, John Doukas, Glenn Noronha and Michael Martin

TargeGen, Inc. 9380 Judicial Drive, San Diego, CA 92121

a) Running title:

NOVEL SRC INHIBITOR TG100435 AND ITS ACTIVE METABOLITE

b) Contact Information of the Corresponding Author:

Steven Xicheng Hu, Ph.D.

TargeGen, Inc., 9380 Judicial Drive, San Diego, CA 92121

Tel.: 1-858-964-2120 Fax: 1-858-678-0762 Email: shu@targegen.com

c) Numerical information of the Manuscript:

The number of Text pages:	29
The number of Tables:	7
The number of Figures:	7
The number of References:	34
The number of Words in the Abstract:	185
The number of Words in the Introduction:	435
The number of Words in the Discussion:	1188

d) Abbreviation Used in the Manuscript:

HPLC, high performance liquid chromatography;

LC/MS/MS, liquid chromatography-triple quadrupole mass spectrometry;

ESI, electrospray ionization;

H-NMR, proton nuclear magnetic resonance spectrometry;

CYP, cytochrome P450

FMO, flavin containing monooxygenase

AUC, area under curve

Abstract

TG100435 is a novel multi-targeted, orally active protein tyrosine kinase (PTK) inhibitor. The inhibition constants (Ki) of TG100435 against Src, Lyn, Abl, Yes, Lck and EphB4 range from 13 to 64 nM. TG100435 has systemic clearance values of 20.1, 12.7 and 14.5 mL/min/kg, and oral bioavailability of 74%, 23% and 11% in mouse, rat and dog, respectively. Four oxidation metabolites of TG100435 have been found in human, dog and rat *in vitro* and *in vivo*. The ethylpyrrolidine *N*-oxide of TG100435 is the predominant metabolite (TG100855) in human, dog and rat. TG100855 is 2-9 times more potent than the parent compound. FMOs are the primary enzymes mediating the biotransformation. Significant conversion of TG100435 to TG100855 has been observed in rat and dog after oral administration. Systemic exposure of TG100855 is 1.1 and 2.1 folds greater than TG100435 in rat and dog after oral dosing of TG100435. Since TG100435 is predominately converted to the more potent *N*-oxide metabolite across species *in vivo* and *in vitro*, the overall tyrosine kinase inhibition in animal models may be substantially increased after oral administration of TG100435.

Introduction

The Src kinase family consists of a group of nonreceptor protein tyrosine kinases (PTKs) including Src, Yes, Fyn, Lyn, Hck, Blk, Brk, Fgr, Frk, Srm, Lck and Yrk (Trevino et al., 2006). Src PTKs play critical roles in a variety of cellular signal transduction pathways regulating diverse processes including cell survival, proliferation, motility, adhesion, and transformation. Elevated or constitutive activation of Src kinase is commonly observed in tumors, most notably in colon and breast cancer, but also occurs in other tumor types, including pancreatic cancer (Lutz et al., 1998). Over-expression of Src PTKs has been associated with tumorigenesis, metastasis, and invasion; consequently, Src family kinases have become very important biological targets in oncological drug development. Small molecule kinase inhibitors have shown great promise as a new class of therapeutics. Most small molecule kinase inhibitors bind at the ATP binding site and exhibit much less toxicity than currently used chemotherapeutic agents (Levitzki and Mishani, 2006).

Nitrogen-containing small molecules are the most common of all of the organic compounds of pharmacological interest. The functionalities of nitrogen provide flexibility in the drug design towards proper potencies and physical properties. However the multiple oxidation states of nitrogen increase the metabolic instability of drug candidates (Cho and Lindeke, 1988). *N*-oxidation is a common biotransformation of aliphatic tertiary amine-containing compounds. The pharmacological and toxicological importance of this metabolic pathway has been widely studied. The nitrogen-centered oxidation of tertiary amine drugs is commonly considered as a detoxification pathway

resulting in non-toxic and biologically inactive metabolites (Carmella et al, 1997; Krueger et al, 2006; Cashman and Zhang, 2006). The benign nature of tertiary amine *N*-oxides under normal physiological conditions has been employed as a prodrug approach to selectively elicit cytotoxic events associated with hypoxic conditions in solid tumor cells (Skálová et al, 2000; Cerecetto and González, 2001; Patterson, 2002). Although *N*-oxidation of the aliphatic tertiary amine-containing drug compounds has been widely identified and studied, the biochemical activity of such *N*-oxide metabolites is not commonly reported.

We report here a novel multi-targeted, orally active PTK inhibitor, TG100435 and its biochemically more potent *N*-oxide metabolite, TG100855. The structural design and activity of TG100435 against human tumor cells have been described elsewhere (Noronha et al, 2006; Noronha et al, 2007). The *N*-oxide metabolite of TG100435 has been identified *in vitro* and *in vivo* in rat and dog in addition to *in vitro* human samples. The biochemical potencies of TG100435 and TG100855 are evaluated for six protein tyrosine kinases. Enzymatic conversion of TG100435 to TG100855 is investigated using mouse liver microsome. The pharmacokinetic properties of TG100435 and TG100855 are also characterized in the mouse, rat and dog.

Materials and methods

Compounds TG100435, ([7-(2,6-Dichloro-phenyl)-5-methyl-benzo[1,2,4]triazin-3-yl]-[4-(2-pyrrolidin-1-yl-ethoxy)-phenyl]-amine) and TG100855, ([7-(2,6-Dichloro-phenyl)-5-methyl-benzo[1,2,4]triazin-3-yl]-{4-[2-(1-oxy-pyrrolidin-1-yl)-ethoxy]-phenyl}-amine) were synthesized at TargeGen, Inc., San Diego, CA (Figure 1). Structures were confirmed by ^{1}H-NMR and mass spectra (Table 1 and 2, Figure 2). For the pharmacokinetic studies, both TG100435 and TG100855 were formulated in 5:5:10:80 of Solutol HS15: PEG400: ethanol: water for intravenous (i.v.) and intraperitoneal (i.p.) administration and formulated in Phosal 50PG® (American Lecithin, Oxford, CT) for oral (p.o.) dosing.

Determination of inhibition constant K_i against a series of kinases K_i values for TG100435 and TG100855 against Src, Lyn, Abl, Yes, Lck and EphB4 were determined using a luminescence-based kinase assay. These recombinant kinases were obtained from Invitrogen, Madison, WI. The assays were performed in 96-well plates at room temperature. Each well contained 40 μL of 75 mM Tris buffer (pH 7.2 containing 95 mM $MgCl_2$, 1.5 mM EGTA, 0.35 mM Triton X-100 and 10 μM β-mercaptoethanol) and an appropriate amount of the PTK was added such that the assay was linear over 60 min. Varying amounts of peptide substrate in water were then added in the presence of a series of different concentrations of either TG100435 or TG100855. The reactions were initiated by addition of ATP to final concentration 3 μM. After 60 min, the reactions were terminated by adding 50 μL of Kinase-Glo reagent (Promega, Madison, WI). Luminosity was measured using an Ultra 384 instrument (Tecan, Charlotte, NC). A

control without peptide substrates was used for a zero point. Enzymatic reaction rates were derived by calculating the difference between kinase catalyzed and noncatalyzed reactions at a specific compound concentration. K_i values were derived from rate data by the noncompetitive enzyme kinetics curve fitting using Prism software (Version 4; GraphPad Software, San Diego CA).

***In vitro* mouse liver microsomal evaluation on *N*-oxidation of TG100435**

Contribution of FMO and CYP to *N*-oxidation of TG100435 in mouse liver microsome was evaluated via heat de-activation of FMO (Grothusen et al., 1996; Cashman, 2005). One set of mouse liver microsomal samples was pre-incubated with a NADPH regenerating system (0.4 mM of NADP, 4.2 mM of glucose-6-phosphate and 1.2 unit/mL of Glucose-6-phosphate dehydrogenase) at 37^{o}C for 1 min then 10 μM of TG100435 was added for continuous incubation. The other set of mouse liver microsomal samples was pre-heated without the NADPH regenerating system at 55^{o}C for 1min then incubated with 10 μM of TG100435 and the NADPH regenerating system at 37^{o}C. The formation of TG100855 was monitored following 0, 10, 20, 30, 45 and 60 min incubation using LC/MS/MS after protein precipitation by cold acetonitrile.

Pharmacokinetic studies of TG100435 and TG100855 Male Sprague-Dawley rats (~300 g), male BALB/c mice (~25 g), and male and female Beagle dogs (~8 kg) were used in the studies. Animals were fasted overnight for single p.o. administration and not fasted for single i.v. or i.p. dosing. Rats were dosed with TG100435 at 25 or 40 mg/kg or TG100855 at 25 mg/kg in the p.o. studies and administered with TG100435 or TG100855 at 5 mg/kg in the i.v. studies. In the i.p. dosing, rats were dosed with

TG100855 at 5 mg/kg. Each dosing group consisted of five rats. Serial blood sampling at 5, 15, 30 min, 1, 3, 6, 24 and 48 hr post-dose for the i.v. dose groups, and at 0.5, 1, 3, 5, 8, 24, 30, and 48 hr post-dose for the p.o. and i.p. dose groups was utilized in order to establish the rat pharmacokinetics. Sodium heparin was used as anti-coagulant in blood samples. The plasma samples were obtained by centrifugation for 10 min.

Mice were dosed with TG100435 at 25 or 30 mg/kg, or TG100855 at 25 mg/kg in the p.o. studies and administered with TG100435 or TG100855 at 5 mg/kg in the i.v. studies. In the i.p. dosing, mice were dosed with TG100855 at 5 mg/kg. Composite blood sampling (n=3 animals per time point) at 5, 15, 30 min, 1, 3, 6, 24 and 48 hr post-dose for the i.v. dose groups, and at 0.5, 1, 3, 5, 8, 24, 30, and 48 hr post-dose for the p.o. and i.p. dose groups was utilized in order to establish the mouse pharmacokinetics.

Dogs were administered TG100435 at 5 mg/kg in the i.v. study or 25 mg/kg in the p.o. study. Each dosing group consisted of two male and two female dogs. Serial blood sampling at 5, 15, 30 min, 1, 3, 7, 12, 24, 36 and 48 hr post-dose for the i.v. dose group and at 0.5, 1, 3, 5, 8, 12, 24, 36 and 48 hr post-dose for the p.o. dose group was utilized in order to establish the dog pharmacokinetics. Dog urine samples were collected from the i.v. study with 12 hr interval at 12 hr, 24 hr, and 48 hr.

Sample preparation for metabolite identification *In vitro samples*: TG100435 (80 μM) was incubated with rat, dog or human liver microsome (*In Vitro* Technologies, Inc., Baltimore, MD, 8 mg protein/mL) in 10 mM phosphate buffer (pH 7.4) in the presence of the NADPH regenerating system for 4 hrs at 37^{o}C. The reactions were terminated by adding cold acetonitrile and the supernatants were concentrated for analysis. Two

controls were prepared: one without the test compound and the other without the NADPH regenerating system.

In vivo samples: plasma was collected from the pharmacokinetic studies of TG100435 in dogs (i.v. and p.o.) and rats (p.o.) as described previously. Aliquots of the plasma samples of dogs and rats collected from different time points were pooled and processed using protein precipitation by adding acetonitrile. The supernatants were concentrated for analysis. Aliquots of the dog urine from different periods in the dog i.v. study were combined and processed as plasma samples by adding acetonitrile. The supernatant was concentrated for analysis.

Metabolite Identification Metabolites were identified using a triple quadrupole LC/MS/MS system. The HPLC system consisted of two Shimadzu LC-10AD pumps, a Shimadzu DGU-3A degasser, a Shimadzu CTO-10A column heater, a Shimadzu SCL-10A controller, an Agilent 1100 series DAD detector and a Leap Technologies CTC HTS autosampler. Samples were separated on a Zorbax SB C-18 (3.5 μm particle size, 50 mm x 2.1 mm) column using a 20 min, 27% to 37% linear gradient of 0.1% formic acid in water and 0.1% formic acid in acetonitrile at a flow rate of 0.25 mL/min and column temperature of 40^{o}C. An API3000 triple quadrupole mass spectrometer (Applied Biosystems, Foster City, CA) was interfaced via an ESI probe with HPLC. Positive modes were used in all of the analyses. Precursor ion scans of 98, 395 and 397 were used as survey scans to determine potential biotransformation at ethylpyrrolidine moiety or methylbenzotriazine core of TG100435 (Figure 2). Mass spectra of metabolites were

obtained using product ion scans. MRM (multiple reaction monitoring) was used to confirm the presence of the metabolites in different samples.

Quantitative analysis of pharmacokinetic samples Plasma samples from mouse, rat and dog were prepared by protein precipitation using acetonitrile containing an internal standard. The supernatants were analyzed using the same LC/MS/MS described above. A Phenomenex Synergi Max-RP column (2 µm particle size, 20 mm x 2.0 mm) was used for separation with a one min, 10% to 100% linear gradient of 0.05% trifluoroacetic acid in water and 0.05% trifluoroacetic acid in acetonitrile. TG100435 and TG100855 were quantitatively monitored using positive mode of MRM of 494.2/98.1 and 510.2/98.1, respectively. Pharmacokinetic parameters were calculated using the WinNonlin (Version 4.01, Pharsight Coporation, Mountain View, CA) program with non-compartmental model analysis and the area under the curve (AUC) was estimated by linear trapezoidal integration.

Results

Identification of *N*-oxide metabolites of TG100435

In positive ion mode, the product ion mass spectrum of TG100435 at m/z 494 $(M+H)^+$ displayed six structurally characteristic fragment ions (Figure 2(a)). The ethylpyrrolidine moiety of TG100435 demonstrated the characteristic fragments of m/z 98, 84 and 71 and the corresponding fragments of m/z 395, 408 and 423 associated with the methylbenzotriazine core. Based on the characteristic mass spectrum, metabolites were identified by determining changes in fragmentation patterns at part B, the ethylpyrrolidine moiety, or part A, the methylbenzotriazine core. The precursor ion scans of the fragments 98, 395 or 397 were used as survey scans to detect possible metabolites. Metabolites M1 to M4 were detected. Using product ion scan, mass fragment patterns of those metabolites were obtained (Table 2).

The metabolite M1 with a mass increase of 16 at ethylpyrrolidine moiety was found in the precursor ion scan of 395 or 98 of all samples *in vitro* and *in vivo.* The fragments 114 and 116 in its product ion mass spectrum indicated a mono-oxidation of TG100435 on ethylpyrrolidine moiety (Figure 2(b)). To confirm the structure of the metabolite, three M+16 standards of TG100435 were synthesized: hydroxylation at dichlorobenzene group, *N*-oxidation at methylbenzotriazine group, and *N*-oxidation at the ethylpyrrolidine (TG100855). Both HPLC retention time and mass spectrum confirmed that M1 was TG100855.

The metabolite M2 with a mass increase of 34 from parent compound was found in the dog p.o. sample using the precursor scan of 98. The product ion mass spectrum

indicated that the addition of mass 34 occurred at part A of the parent compound because the fragment pattern of m/z 98, 84 and 71 remained and the m/z 395 and 423 shifted two units to m/z 393 and 421 (Table 2). The metabolite M3 with a mass increase of 50 from parent compound was detected in the rat liver microsomal sample. Its product ion mass spectrum gave a similar fragment pattern as M2 but had fragments 116 and 114 indicating *N*-oxidation at the ethylpyrrolidine moiety. The metabolite M4 with a mass increase of 32 from parent compound was found in the *in vivo* dog p.o. sample. Its product ion mass spectra indicated the addition of two oxygen atoms at the ethylpyrrolidine moiety. The fragments 112 and 130 in the mass spectrum indicated oxidative ring-opening of the pyrrolidine ring.

The presence of these metabolites in each sample was confirmed using MRM method to analyze all of *in vitro* and *in vivo* samples. The metabolites identified in the *in vitro* and *in vivo* samples are listed in Table 3. Oxidation was the major metabolic biotransformation for TG100435 in human, dog and rat. This oxidation occurred at both part B, the ethylpyrrolidine moiety, and part A, the methylbenzotriazine core of the parent compound.

M1 was the only metabolite detected in trace amount in human liver microsomal sample using mass spectrometry. M1 was the predominant metabolite in the rat liver microsomal, rat and dog *in vivo* samples detected at 190-400 nm of photodiode array (Figure 3(a) and (b)). M4 was also present in *in vivo* dog samples but at a reduced level compared to M1 (Figure 3(b)).

Enzymatic potency of TG100435 and TG100855

TG100435 displayed biochemical potency against Src, Lyn, Abl, Yes, Lck and EphB4 with K_i values ranging from 13 to 64 nM (Table 4). Since TG100855 was the predominant metabolite of TG100435, a synthetic standard was generated and its kinase inhibition constants were determined (Table 4). Compared with TG100435, TG100855 was 2 to 9 times more potent against the same set of PTKs.

***N*-oxidation of TG100435 in *in vitro* study**

Contribution of FMO and CYP on the *N*-oxidation of TG100435 was distinguished by de-activating FMO through pre-heating mouse liver microsome without NADPH. Compared with the non-heated mouse liver microsomal system, the initial formation rate of TG100855 was reduced significantly (Figure 4).

Pharmacokinetics of TG100435 and its active metabolite TG100855 in mouse, rat and dog

Pharmacokinetic parameters of TG100435 and TG100855 after single doses in mouse, rat, and dog are listed in Table 5, 6 and 7. After single bolus injection of 5 mg/kg of TG100435, the compound showed low to moderate systemic clearance, large volume of distribution, and long half life in all tested animals. Oral bioavailability of TG100435 was high in mouse but low in rat and dog. Absorption of TG100435 was slow in those animals, as peak plasma levels were reached at 5-8 hr.

Formation of TG100855 was monitored in the oral studies of TG100435 in mouse, rat and dog. Significant amount of TG100855 was formed after a single oral administration of 25 or 30 mg/kg of TG100435 in either dog or rat (Figure 5(b and c)) but much less was

detected in mouse after a single oral dosing of 40 mg/kg of TG100435 (Figure 5(a)). The AUC ratios of TG100855 to TG100435 were 2.1, 1.1 and 0.38 in dog, rat and mouse, respectively.

Following a single i.v. dose of TG100855 in mouse and rat, TG100855 showed similar clearance as its parent compound in rat but lower clearance in mouse. Its volume of distribution and half life were much less than its parent compound in both mouse and rat. TG100855 was partially converted back to TG100435 after dosing in different routes. There was no significant difference in mean AUC values of TG100855 and the converted TG100435 following i.v. and i.p. doses in both mouse and rat. Oral bioavailability of TG100855 was low in both animals but its oral absorption was more rapid than TG100435, as peak plasma levels were reached at 1 and 3.5 hr for mouse and rat, respectively. After oral administration of TG100855, the mean AUC of the converted TG100435 was larger than those of TG100855. The AUC ratios of the converted TG100435 to TG100855 were 1.93 and 1.87 in rat and mouse, respectively. The bioavailability by converting TG100435 back to TG100855 was counted to 6.8% and 3.1%. Mean plasma concentration-time profiles obtained from both intravenous and oral dosing of TG100435 or TG100855 in mouse and rat are demonstrated in Figure 6 and 7. The intravenously administered compounds declined biexponentially in both animals.

Discussion

Oxidation is the primarily observed metabolic process of TG100435 *in vitro and in vivo*. *N*-oxidation at the tertiary amine of the ethylpyrrolidine moiety (M1, TG100855) has been found in all samples of the study. This metabolite is the predominant metabolite in rat and dog, and the only one observed in the human liver microsomal sample. *N*-oxidation of either aliphatic or aromatic amines by microsomal enzymes is well documented. For example, the *N*-oxides of the aliphatic amines in tamoxifen (Foster et al., 1980), imipramine (Bickel, 1972), the imipramine-related compounds amitryptyline (Beckett, 1971), chloropromazine (Bickel, 1972) and *N*,*N*-dimethyl-^{5}H-dibenzo-[a,d]cycloheptene-Δ^{5},γ-propylamine (Belvedere et al., 1974) are well established. *N*-oxidation is mediated by both cytochrome P450 and FMO (Miwa and Walsh, 1988). It has been found that *N*-oxidation of a potent 5-HTID receptor agonist, L-755,606 was mediated primarily by FMO3 while CYP had minimal involvement in the *N*-oxidative pathway in human (Prueksaritanont et al., 2000). FMO3 is also the most active isoform in *N*-oxidation of trimethylamine in human (Lang et al., 1998). It has been demonstrated that *N*-oxidation of tamoxifen in human was catalyzed by FMO1 and FMO3 (Parte and Kupfer, 2005). On the other hand, *N*-oxidation of capravirine, a non-nucleoside reverse transcriptase inhibitor, is mediated predominantly by CYP3A4 in human liver microsome (Bu et al., 2006). Our studies indicate that *N*-oxidation of TG100435 is primarily mediated by FMO (Figure 4).

The mass spectra of M2 and M3 do not provide sufficient information to propose structures due to the low concentrations observed in the study. These low concentrations

may result in artificial mass spectra. Metabolite M2 appears to possess a 34 amu increase associated with part A of the parent molecule. M3 appears to be a combination of M1 and M2. Metabolite M4 is proposed as the oxidized ring-opening ethylpyrrolidine metabolite. Similar ring-opening metabolites at the pyrrolidine ring have been identified in a variety of studies, such as in levormeloxifene (Mountfield et al., 2000), bepridil (Wu et al., 1992) and prolintane (Rucker et al., 1992). It is proposed that the ring-opening metabolites are formed through alicyclic hydroxylation at the α-C of the pyrrolidine ring (Wu et al, 1988). The absolute structural assignments of M2 through M4 require further investigation.

TG100435 is a potent multi- tyrosine kinase inhibitor. Its *N*-oxide metabolite TG100855 is even more potent biochemically than its parent compound. Only a few *N*-oxide metabolites of drug compounds have been reported to have high potency. For example, the *N*-oxide metabolite of roflumilast shows equal potency to its parent compound in attenuating allergen-induced bronchoconstriction in guinea pigs (Bundschuh et al., 2001). The *N*-oxide of a drug is usually less active than its parent compound. Many *N*-oxide metabolites are found to be not active. For example, the *N*-oxide of an antitumor agent, azonafide is much less potent and cytotoxic than its parent compound (Uematsu et al, 1989). The *N*-oxides are rapidly excreted out in the urine since FMO generally converts nucleophilic heteroatom-containing chemicals and drugs into harmless, polar, readily excreted metabolites (Cashman and Zhang, 2006). Therefore *N*-oxidation is often considered as a detoxication mechanism for tertiary nitrogen containing drugs. High potency of TG100855 against multi- tyrosine kinases

presents a quite different potential of *N*-oxide metabolites. Because the *N*-oxidation of TG100435 results in a much more potent metabolite, this metabolism will not decrease but potentially maintain or even increase inhibition to tyrosine kinases.

The pharmacokinetic profile of TG100435 has been determined in mouse, rat and dog. TG100435 has low or moderate clearance in those species compared to hepatic blood flow. However the oral bioavailability of TG100435 is much lower in rat and dog than in mouse. The low oral bioavailability is a result of significant *N*-oxidation of TG100435 in rat and dog. It has been reported that male rat liver microsome contains twice of the amount of FMO3 than male mouse liver microsome (Ripp et al, 1999). This is consistent with our observation that there is more conversion of TG100435 to TG100855 in male rat liver microsome than in male mouse liver microsome (data not shown). On account of the fact that much more TG100435 is *N*-oxidized in rat and dog; the observed oral bioavailability of TG100435 is much lower in rat and dog than in mouse. If the converted TG100855 is accounted, the overall oral availability of active compounds (TG100435 plus TG100855) would be increased to about 30% or 50% in dog or rat. Moreover because TG100855 is 2-9 times more potent than its parent compound, the overall effect of inhibition to Src kinases in rat and dog will be equivalent to or even greater than in mouse after oral dosing.

TG100855 has similar or lower clearance in rat and mouse as TG100435. The oral bioavailability of this metabolite is very low in both mouse and rat although TG100855 is more potent. After both i.v. and p.o. dosing of TG100855, TG100855 is partially converted back to TG100435 in both mouse and rat. The back conversion is more

evident in oral administrations. Since i.p. administration of TG100855 exhibits complete bioavailability in mouse and >80% bioavailability in rat (Table 5 and 6), the intestinal first-pass metabolism may be the primary contributor for the back conversion. Back conversion of metabolites to parent compounds is not uncommon and has been found between several drug compounds and their metabolites in rat (Ebling and Jusko, 1986; Kuo et al., 1993; Wong et al., 1996). The reduction of tertiary amine *N*-oxides through different enzymes has been extensively documented. It is believed that cytochrome P450 is partly responsible for *N*-oxide reduction and this reduction appears to be relatively nonspecific with respect to substrate structures (Cho, 1988; Skálová et al, 2000).

The role of pharmacologically active metabolites is a concern in drug discovery and development. Active metabolites can contribute significantly to the overall therapeutic and adverse effects of drugs. To fully understand the mechanism of action of drugs, it is important to recognize the biotransformation and pharmacokinetics of active metabolites. TG100855 has much higher biochemical potency than its parent compound but its oral bioavailability is poor. This makes TG100855 inappropriate as an oral drug. However, its parent compound, TG100435 has reasonably high overall oral bioavailability (TG100435 plus TG100855) and converts predominantly to TG100855 *in vitro* and *in vivo*. As a result, after *in vivo* oral administration of TG100435 the overall exposure of TG100435 and TG100855 is high. Because TG100435 converts to the more potent metabolite, this may potentially increase overall inhibition to PTKs thus affect efficacy of TG100435 in *in vivo* models. A further investigation of this is needed.

In summary, TG100435 is a novel multi-targeted protein tyrosine kinase inhibitor. This small molecule inhibitor has low to moderate systemic clearance in mouse, rat and dog. The oral bioavailability of TG100435 is high in mouse but low in rat and dog. The low bioavailability in rat and dog is due to significant biotransformation of TG100435 to its metabolite TG100855. TG100855 is 2 to 9 times more potent than its parent compound. Since TG100435 is predominately converted to the more potent *N*-oxide metabolite across species *in vivo* and *in vitro*, the overall tyrosine kinase inhibition in animal models may be substantially increased after oral administration of TG100435.

Acknowledgements

The authors would like to acknowledge Juliet Chin, Jann Key, Silva Stoughton, and Cyrus Virata for their contributions.

References

Beckett AH (1971) Metabolic oxidation of aliphatic basic nitrogen atoms and their alpha-carbon atoms. *Xenobiotica* **1**: 365-383.

Belvedere G, Rovei V, Pantarotto C and Frigerio A (1974) Mass spectrometric identification of an N-oxide formed by incubation of N,N-dimethyl-^{5}H-dibenzo-[a,d]cycloheptene-Δ^{5},γ-propylamine with rat liver microsomes. *Biomed Mass Spec* **1**: 329-331.

Bickel MH (1972) Liver metabolic reactions: tertiary amine N-dealkylation, tertiary amine N-oxidation, N-oxide reduction, and N-oxide N-dealkylation. I. Tricyclic tertiary amine drugs. *Archs Biochem Biophys* **148**: 54-62.

Bu HZ, Zhao P, Kang P, Pool WF and Wu EY (2006) Identification of enzymes responsible for primary and sequential oxygenation reactions of capravirine in human liver microsomes. *Drug Metab Dispos* **34**:1798-1802

Bundschuh DS, Eltze M, Barsig J, Wollin L, Hatzelmann A and Beume R (2001) In vivo efficacy in airway disease models of roflumilast, a noval orally active PDE4 inhibitor. *J Pharmacol Exp Ther* **297**: 280-290

Carmella SG, Borukhova A, Akerkar SA and Hecht SS (1997) Analysis of human urine for pyridine-N-oxide metabolites of 4-(methylnitrosamino)-1-(3-pyridyl)-1-butanone, a tobacco-specific lung carcinogen Cancer. *Epidemiol Biomarkers Prev* **6**: 113-120

Cashman, JR (2005) Some distinctions between flavin-containing and cytochrome P450 monooxygenases. *Biochem Biophys Res Commun*. **338**: 599-604.

Cashman, JR and Zhang J (2006) Human flavin-containing monooxygenases. *Annu Rev Pharmacol Toxicol* **46**: 65-100

Cerecetto H and Gonzalez M (2001) N-oxides as hypoxia selective cytotoxins. *Mini Rev. Med. Chem* **1**: 219-231

Cho AK (1988) Metabolic disposition of nitrogen functionalities. *Prog Bas Clin Pharmac* **1**: 184-212.

Cho AK and Lindeke B (1988) *Biotransformation of Organic Nitrogen Compounds.* Karger, Basel

Ebling WF and Jusko WJ (1986) The determination of essential clearance, volume, and residence time parameters of recirculating metabolic systems: the reversible metabolism

of methyprednisolone and methylprednisone in rabbits. *J Pharmacokinet Biopharm* **14**: 557-599.

Foster AB, Griggs LJ, Jarman M., Van Maanen JMS and Schulten HR (1980) Metabolism of Tamoxifen by rat liver microsomes: formation of the N-oxide, a new metabolite. *Biochem Pharmacol* **29**: 1977-1979.

Grothusen A, Hardt J, Brautigam L, Lang D, Bocker R (1996) A convenient method to discriminate between cytochrome P450 enzymes and flavin-containing monoxygenases in human liver microsomes. *Arch Toxicol* **71**: 64-71

Krueger SK, Vandyke JE, Williams DE and Hines RN (2006) The role of flavin-containing monooxygenase (FMO) in the metabolism of tamoxifen and other tertiary amines. *Drug Metab Rev* **38**:139-47.

Kuo BS, Poole JC, Hwang KK and Cheng H (1993) Pharmacokinetics and metabolic interconversion of intravenous 4-amino-5-chloro-2-[(methylsulfinyl)ethoxy]-N-[2-(diethylamino)ethyl]benzamide and its sulfide and sulfone metabolites in rats. *J Pharm Sci* **82**: 694-698.

Lang DH, Yeung CK, Peter RM, Ibarra C, Gasser R, Itagaki K, Pilpot RM and Rettie AE (1998) Isoform specificity of trimethylamine N-oxygenation by human flavin-containing

monooxygenase (FMO) and P450 enzymes: selective catalysis by FMO3. *Biochem Pharmacol* **56**: 1005-1012

Levitzki A and Mishani E (2006) Tyrphostins and other Trosine kinase inhibitors. *Annu Rev Biochem* **75**: 93-109.

Lutz MP, Silke Eβer IB, Flossmann-Kast BBM, Vogelmann R, Lührs H, Friess H, Büchler MW and Adler G (1998) Overexpression and activation of the tyrosine kinase Src in human pancreatic carcinoma. *Biochem Biophys Res Commun* **243**: 503-508.

Miwa GT and Walsh JS. (1988) Cytochrome P450 in nitrogen metabolism. *Pro Bas Clin Pharmac* **1**: 27-62.

Mountfield RJ, Kiehr B and John BA (2000) Metabolism, disposition, excretion, and pharmacokinetics of levormeloxifene, a selective estrogen receptor modulator in the rat. *Drug Metab Dispos* **28**: 503-513.

Noronha G, Barrett K, Cao J, Dneprovskaia E, Fine R, Gong X, Gritzen C, Hood J, Kang X, Klebansky B, Li G, Liao W, Lohse D, Mak CC, McPherson A, Palank MSS, Pathak VP, Renick J, Soll R, Splittgerber U, Wrasidlo W, Zeng B, Zhao N and Zhou Y (2006) Discovery and preliminary structure-activity relationship studies of novel benzotrianzine based compounds as Src inhibitors. *Bioorg Med Chem Lett* **16**: 5546-5550

Noronha G, Barrett K, Boccia A, Brodhag T, Cao J, Chow CP, Dneprovskaia E, Doukas J, Fine R, Gong X, Gritzen C, Gu H, Hanna E, Hood JD, Hu S, Kang X, Key J, Klebansky B, Kousba A, Li G, Lohse D, Mak CC, McPherson A, Palank MSS, Pathak VP, Renick J, Shi Feng, Soll R, Splittgerber U, Stoughton S, Tang S, Yee S, Zeng B, Zhao N and Zhu H (2007) Discovery of [7-(2,6-Dichlorophenyl)-5-methyl-benzo[1,2,4]triazin-3-yl]-[4-(2-pyrrolidin-1-yl-ethoxy)phenyl] amine---a potent, orally active Src kinase inhibitor with anti-tumor activity in preclinical assays. *Bioorg Med Chem Lett* **17**:602-608

Parte P and Kupfer D (2005) Oxidation of tamoxifen by human flavin-containing monooxygenase (FMO) 1 and FMO3 to tamoxifen-N-oxide and its novel reduction back to tamoxifen by human cytochromes P450 and hemoglobin. *Drug Metab Dispos* **33**: 1446-1452.

Patterson LH (2002) Bioreductively activated antitumor N-oxides: the case of AQ4N, a unique approach to hypoxia-activated cancer chemotherapy. *Drug Metab Rev* **34**:581-592.

Prueksaritanont T, Lu P, Gorham L, Sternfeld F and Vyas KP. (2000) Interspecies comparison and role of human cytochrome P450 and flavin-containing monooxygenase

in hepatic metabolism of L-775,606, a potent 5-HT_{ID} receptor agonist. *Xenobiotica* **30**: 47-59.

Ripp SL, Itagaki K, Philpot RM and Elfarra AA (1999) Species and sex differences in expression of flavin-containing monooxygenase form 3 in liver and kidney microsomes. *Drug Metab Dispos* **27**: 46-52.

Rucker G, Neugebauer M and Zhong D (1992) Study on the metabolism of racemic prolintane and its optically pure enantiomers. *Xenobiotica* **22**: 143-152.

Skálová L, Nobilis M, Szotáková B, Wsól V, Kubíček V, Baliharová V and Kvasničková E (2000) Effect of substituents on microsomal reduction of benzo(c)fluorine N-oxides. *Chem Biol Interact* **126**:185-200.

Trevino JG, Summy JM and Gallick GE (2006) Src inhibitors as potential therapeutic agents for human cancers. *Mini Rev. Med. Chem.* **6**: 109-120.

Uematsu T, Sato R, Vozeh S, Follath F and Nakashima M (1989) Relative electrophysiological potencies of quinidine, 3-hydroxyquinidine and quinidine-N-oxide in guinea pig heart. *Arch Int Pharmacodyn* **297**: 29-38

Wong YN, Quon CY, Holm KA, Burcham DL, Frey NL, Huang SM and Lam GN (1996)

Pharmacokinetics and metabolism of EXP921, a novel cognitive enhancer, in rats. *Drug Metab Dispos* **24**: 172-179.

Wu WN, Hills JF, Chang SY and Ng KT (1988) Metabolism of bepridil in laboratory animals and humans. *Drug Metab Dispos* **16**: 69-77.

Wu WN, Pritchard JF, Ng KT, Hilis JF, Uetz JA, Yorgey KA., Mckown LA and O'Neill PJ (1992) Disposition of bepridil in laboratory animals and man. *Xenobiotica* **22**: 153-169.

Legends for figures

Figure 1. Chemical structures of (a) TG100435 and (b) TG100855 (Proton chemical shift is listed in Table 1)

Figure 2. Product ion mass spectra and fragment patterns of (a) TG100435 (molecular ion m/z 494) and (b) its active metabolite TG100855 (molecular ion m/z 510)

Figure 3. Chromatograms of (a) rat p.o. and (b) dog p.o. samples at UV (190-400nm) (metabolite peaks were determined by comparing with controls. The retention time of TG100435 is 14.1 min)

Figure 4. Effect of FMO on formation of TG100855 in mouse liver microsome. (●) The mouse liver microsome was pre-heated at 55 ^{o}C for 1 min without NADPH before addition of TG100435 and NADPH; (□) the mouse liver microsome was incubated with NADPH at 37 ^{o}C for 1 min before addition of TG100435. TG100855 was monitored at each time point of three replicates. The concentration is expressed using peak area ratio of TG100855 to an internal standard.

Figure 5. (a) plasma concentration vs. time profile of TG100435 (□) and TG100855 (♦) after 40 mg/kg oral dose of TG100435 in mouse ($AUC_{(0\text{-}inf)}$: 35100 hr • ng/mL for TG100435 and 13400 hr • ng/mL for TG100855); (b) Plasma concentration vs. time profile of TG100435 (□) and TG100855 (♦) after 30 mg/kg oral dose of TG100435 in rat ($AUC_{(0\text{-}inf)}$: 8120 hr • ng/mL for TG100435 and 9310 hr • ng/mL for TG100855); (c)

Plasma concentration vs. time profile of TG100435 (□) and TG100855 (♦) after 25 mg/kg oral dose of TG100435 in dog ($AUC_{(0\text{-}inf)}$: 3109 hr • ng/mL for TG100435 and 6470 hr • ng/mL for TG100855);

Figure 6. (a) Plasma concentration vs. time profile of TG100435 (○), TG100855 (■) and the converted TG100435 (Δ) after 5 mg/kg intravenous dose of TG100435 or TG100855 in mouse; (b) plasma concentration vs. time profile of TG100435, TG100855 and the converted TG100435 after 25 mg/kg oral dose of TG100435 or TG100855 in mouse

Figure 7. (a) Plasma concentration vs. time profile of TG100435 (○), TG100855 (■) and the converted TG100435 (Δ) after 5 mg/kg intravenous dose of TG100435 or TG100855 in rat; (b) plasma concentration vs. time profile of TG100435, TG100855 and the converted TG100435 after 25 mg/kg oral dose of TG100435 or TG100855 in rat.

TABLE 1

^{1}H NMR of TG100435 and TG100855 in DMSO-d_6 (500 MHz)

TG100435	δ (ppm)	1.68		2.52		2.64	2.78	4.07	7.00	7.50	7.6-7.7	7.94	8.06	10.86
	No. of H*	4H (a)		4H (b)		3H (c)	2H (d)	2H (e)	2H	1H	3H	2H	1H	1H
	multiplet	br. s		br. s		s	br. s	t	d	t	m	d	t	s
	(*J*, Hz)							(6.0)	(9.1)	(8.2)		(9.1)	(1.6)	
TG100855	δ (ppm)	1.99	2.13	3.47	3.55	2.62	3.80	4.51	7.06	7.51	7.6-7.7	7.96	8.06	10.89
	No. of H*	2H (f)	2H (f)	2H (g)	2H (g)	3H (h)	2H (i)	2H (j)	2H	1H	3H	2H	1H	1H
	multiplet	br. s	br. s	br. s	br. s	s	br. s	t	d	t	m	d	t	s
	(*J*, Hz)							(4.6)	(9.1)	(8.2)		(9.0)	(1.6)	

Note: δ – chemical shift, H – proton, br. – broad, s – singlet, d – doublet, t – triplet, J – coupling constant
**a-j: position of protons labeled in Figure 1*

TABLE 2

Molecular ions and fragment ions of TG100435 and its metabolites

Compound	Molecular ion	Fragment ions
TG100435	494	423, 408, 395, 367, 98, 84, 71
M1 (TG100855)	510	423, 395, 367, 116, 114, 98, 84, 71
M2	528	492, 421, 406, 393, 98, 84, 71
M3	544	421, 393, 116, 114, 98, 84
M4	526	423,408, 399, 397, 368, 130, 112, 87

TABLE 3

Metabolites of TG100435 identified in rat, dog and human

Metabolite	M	RT* (min)	Dog liver microsome	Human liver microsome	Rat liver microsome	Rat p.o.	Dog p.o.	Dog i.v.	Dog urine
M1	M+16	15.2	+	+	+	+	+	+	+
M2	M+34	6.3	+	-	+	+	+	-	-
M3	M+50	7.1	-	-	+	-	-	-	-
M4	M+32	12.3	+	-	-	+	+	+	-

**RT—retention time. "+" and "-"—found and not found.*

TABLE 4

Inhibition constants of TG100435 and TG100855 to different protein tyrosine kinases

PTK	Ki (nM, TG100435)	Ki (nM, TG100855)
Src	28.1 ± 2.1	7.22 ± 2.46
Lyn	25.9 ± 1.2	4.19 ± 0.66
Abl	19.4 ± 3.5	2.04 ± 0.28
Yes	12.9 ± 1.9	5.97 ± 0.43
Lck	29.4 ± 3.4	11.7 ± 1.6
EphB4	63.8 ± 5.2	7.27 ± 0.55

TABLE 5

Mean (S.D.) PK parameters of TG100435 and TG100855 following 5 mg/kg i.v. and i.p. dosing in mice and rats

Species	Route	Compound	C_0 (ng/mL)	AUC $_{(0-\infty)}$ (ng • hr/mL)	$t_{1/2}$ (hr)	Vd (L/kg)	CL (mL/min/kg)	AUC* $_{(0-\infty)}$ (ng • hr/mL)
	i.v.	TG100435	873	4140	5.4	9.4	20.1	-
Mouse	i.v.	TG100855	9030	5350	0.9	1.2	15.6	1390
	i.p.	TG100855	4100	6520	2.8	2.6	11.6	1400
	i.v.	TG100435	1650 (840)	7030(2170)	8.9(1.9)	9.4(1.7)	12.7(3.5)	
Rat	i.v.	TG100855	12200(3980)	6050(386)	1.6(0.2)	1.9(0.4)	13.8(0.9)	539(171)
	i.p.	TG100855	1080(806)	4990(577)	2.3(1.4)	3.3(2.3)	17.0(2.0)	498(62)

**AUC of TG100435 converted from TG100855 after dosed with TG100855*

TABLE 6

Mean (S.D.) PK parameters of TG100435 and TG100855 following 25mg/kg p.o. administration in mice and rats

Species	Compound	C_{max} (ng/mL)	t_{max} (hr)	AUC $_{(0-\infty)}$ (ng • hr/mL)	AUC $_{(0\text{-last})}$ (ng • hr/mL)	F %
Mouse	TG100435	618	8	15300	15000	74
	TG100855	171	1	939	912	3.5
	TG100435[#]	113	7	1760	1740	6.8*
Rat	TG100435	348(82)	8	8010(3850)	7980(3810)	23
	TG100855	160(85)	3.5(1.9)	470(145)	467(150)	1.6
	TG100435[#]	73.0(31.8)	4.0(2.0)	906(437)	881(431)	3.1*

 # TG100435 converted from TG100855 after dosed with TG100855
**Oral bioavailability from the converted TG100435*

Table 7

Mean (S.D.) PK parameters of TG100435 and TG100855 following 5 mg/kg i.v. and 25 mg/kg p.o. administration in dogs

Route	Compound	C_0 (ng/mL)	$t_{1/2}$ hr	AUC $_{(0-\infty)}$ (ng • hr/mL)	Vd (L/kg)	CL (mL/min/kg)	
i.v.	TG100435	1660(335)	15.1(1.6)	5800(158)	18.7(2.2)	14.5(0.4)	
Route	Compound	C_{max} (ng/mL)	t_{max} (hr)	AUC $_{(0-\infty)}$ (ng • hr/mL)	AUC $_{(0\text{-last})}$ (ng • hr/mL)	F %	AUC* $_{(0-\infty)}$ (ng • hr/mL)
p.o.	TG100435	102(11)	4.0(1.0)	3109(812)	2536(502)	10.7	6470(2630)

**AUC of TG100855 converted from TG100435 (Same p.o. study of Figure5(c))*

Figure 1

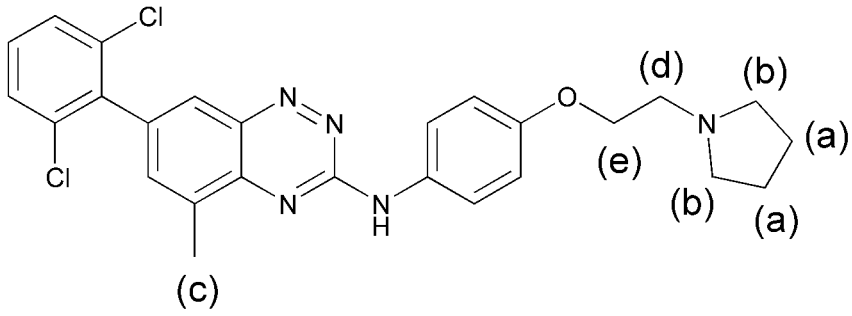

(a) TG100435

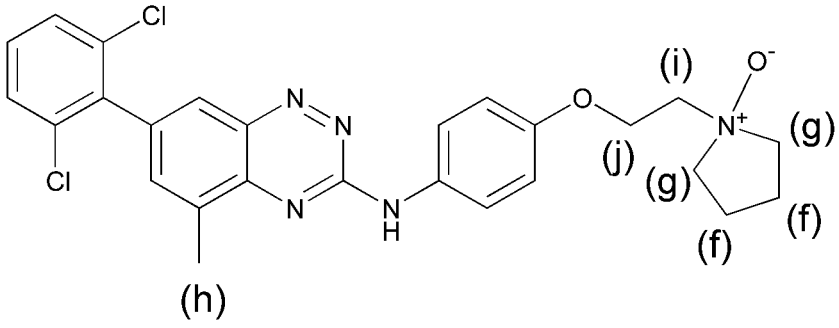

(b) TG100855

Figure 2

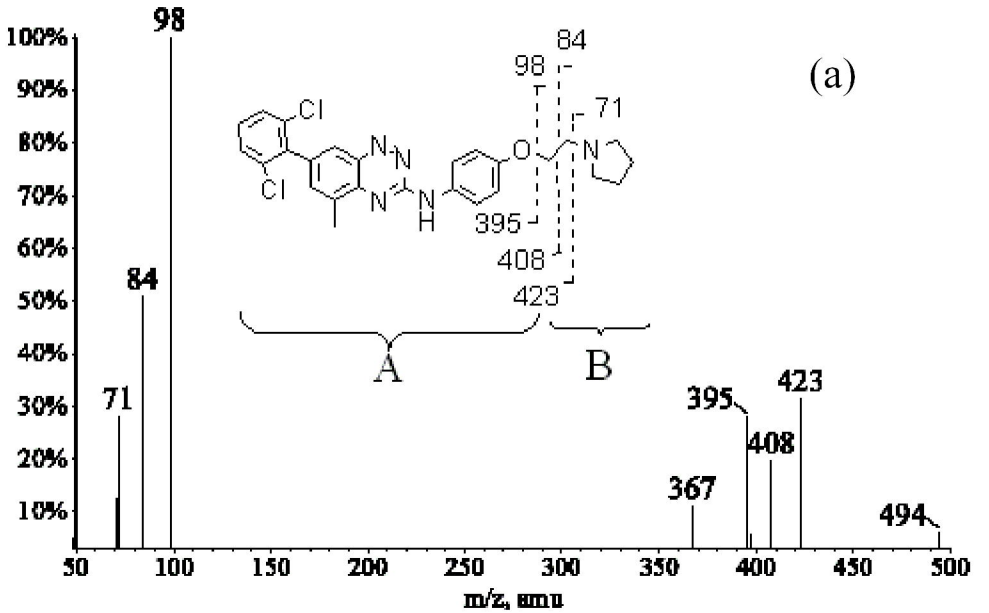
(a)
98
84
71
395
408
423
A
B
367
494
m/z, amu

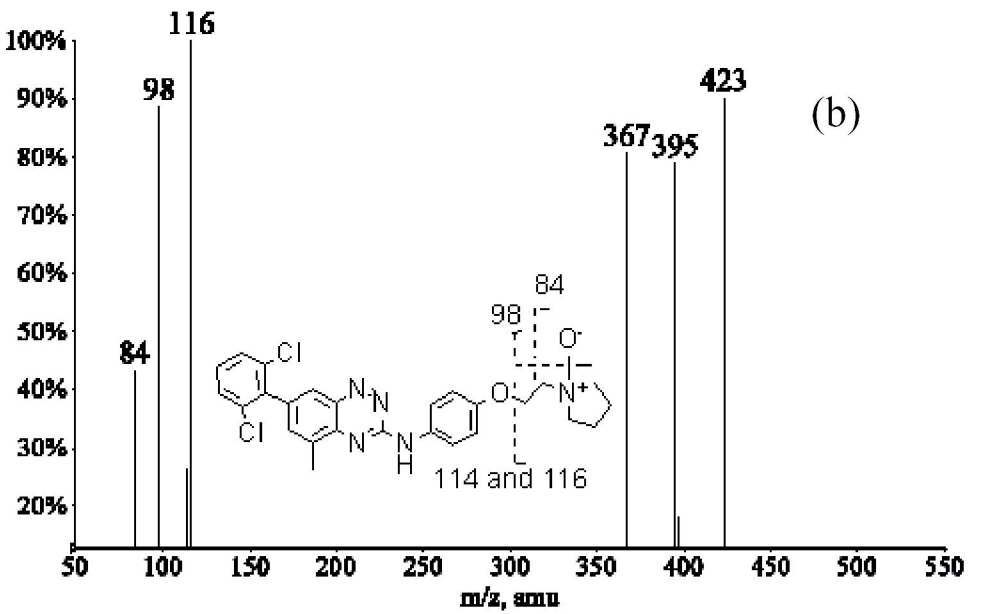
(b)
116
98
84
423
367
395
114 and 116
m/z, amu

Figure 3

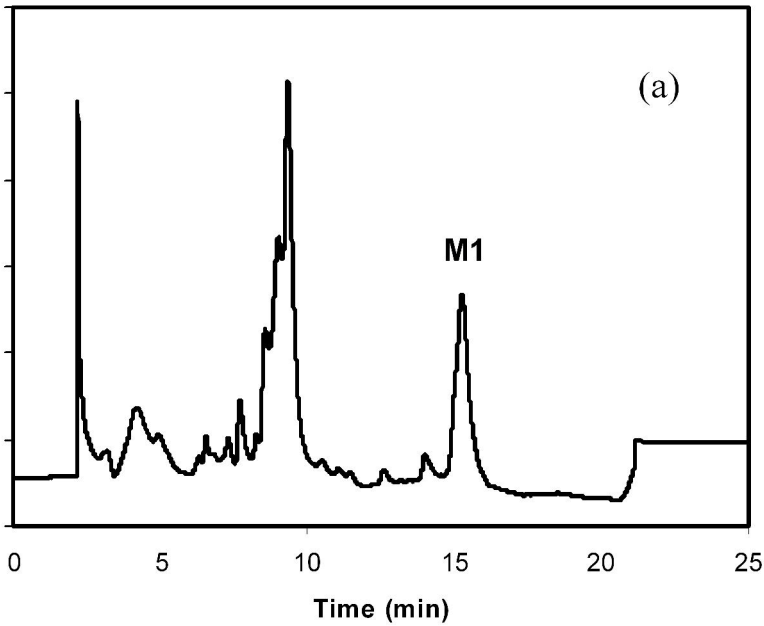

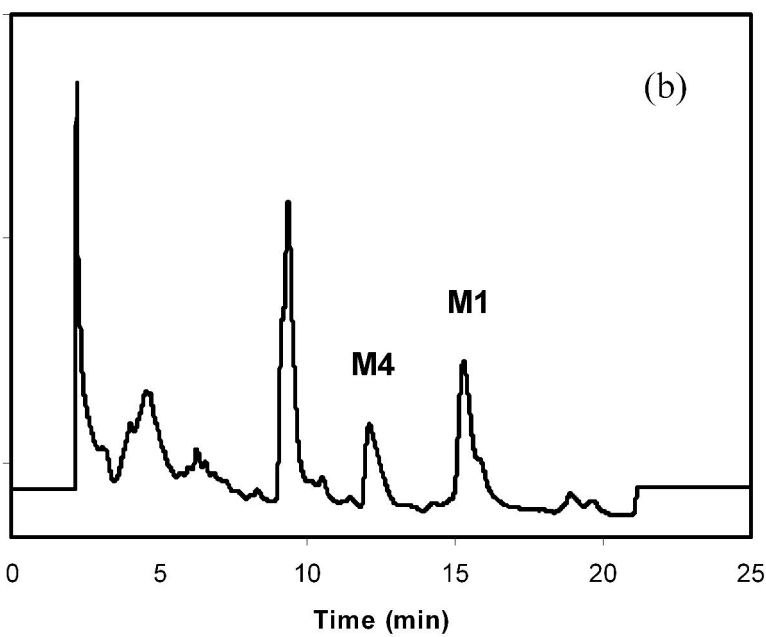

Figure 4

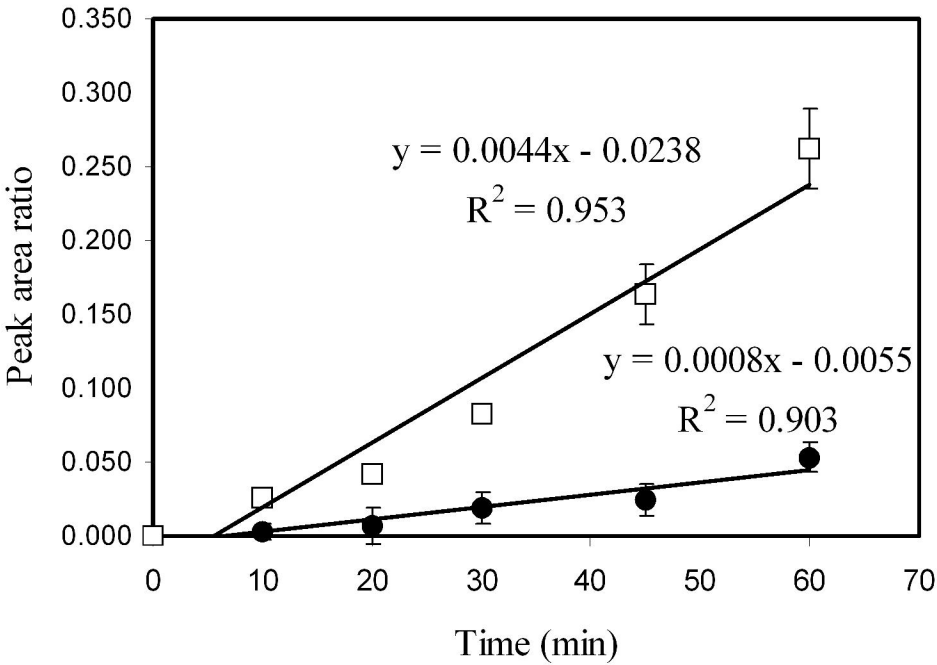
0.350
0.300
0.250
0.200
0.150
0.100
0.050
0.000
Peak area ratio
y = 0.0044x - 0.0238
R2 = 0.953
y = 0.0008x - 0.0055
R2 = 0.903
0
10
20
30
40
50
60
70
Time (min)

Figure 5

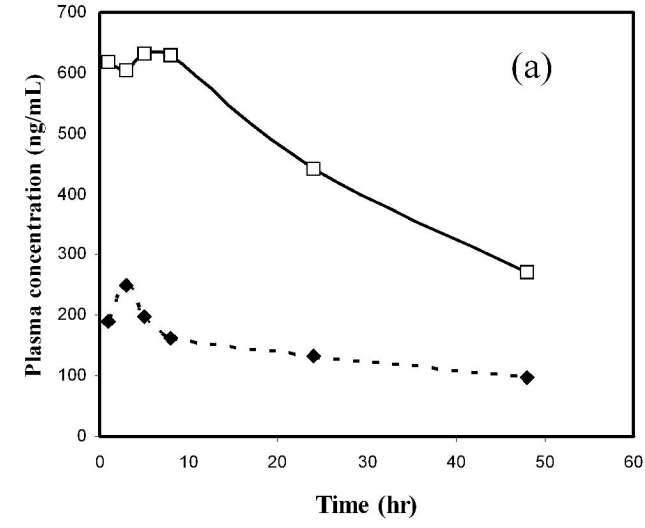
(a)
Plasma concentration (ng/mL)
Time (hr)
0
100
200
300
400
500
600
700
0
10
20
30
40
50
60

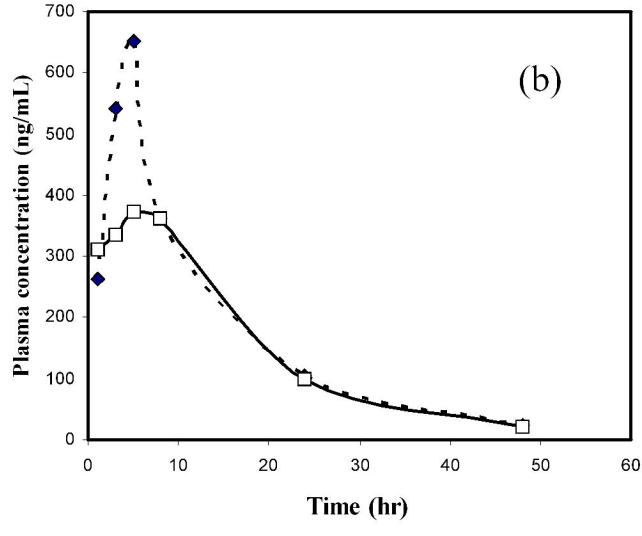
(b)
Plasma concentration (ng/mL)
Time (hr)
0
100
200
300
400
500
600
700
0
10
20
30
40
50
60

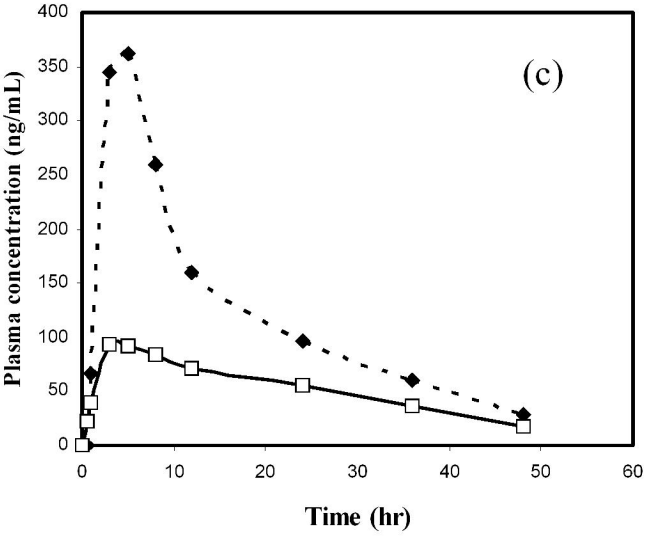
(c)
Plasma concentration (ng/mL)
Time (hr)
0
50
100
150
200
250
300
350
400
0
10
20
30
40
50
60

Figure 6

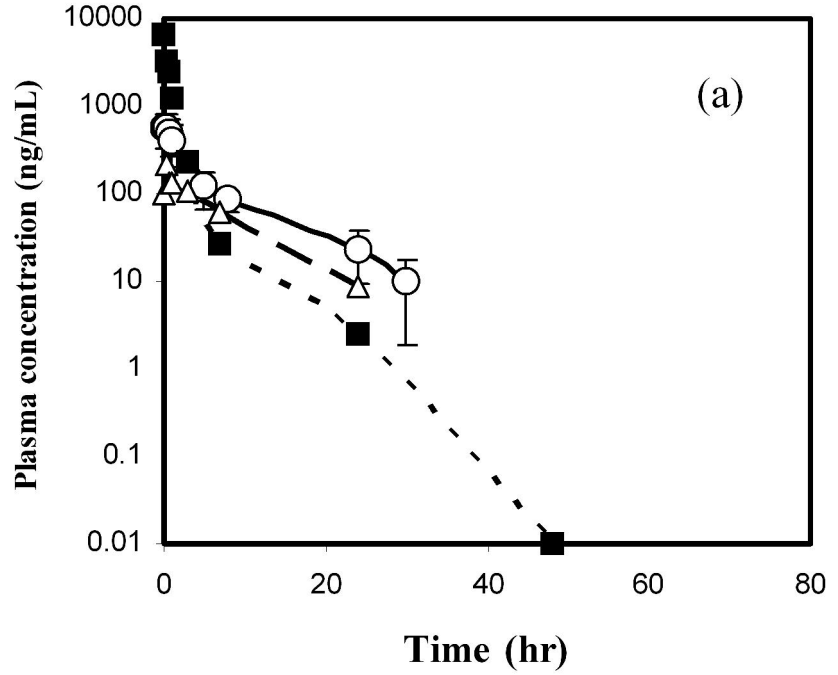
10000
1000
100
10
1
0.1
0.01
Plasma concentration (ng/mL)
(a)
0
20
40
60
80
Time (hr)

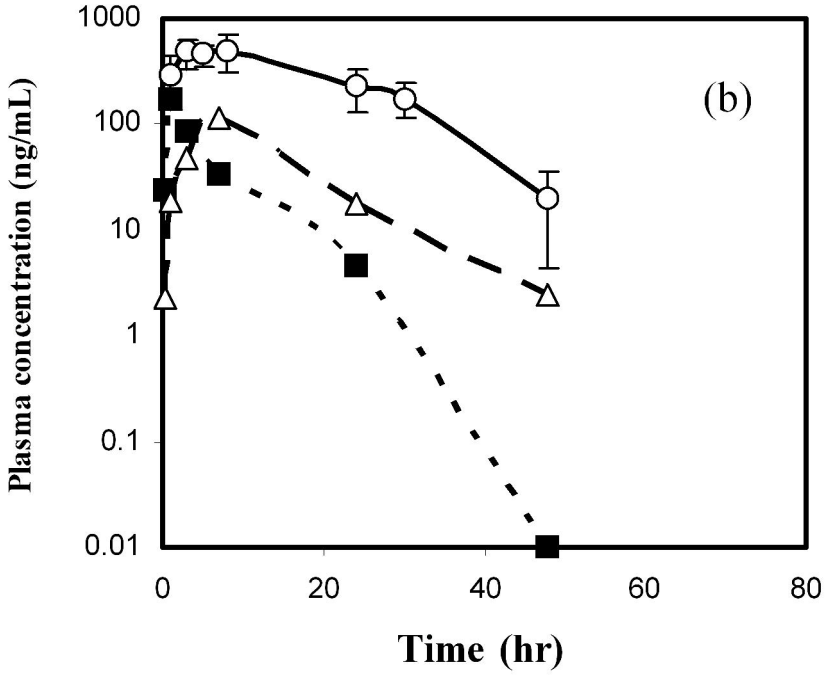
1000
100
10
1
0.1
0.01
Plasma concentration (ng/mL)
(b)
0
20
40
60
80
Time (hr)

Figure 7

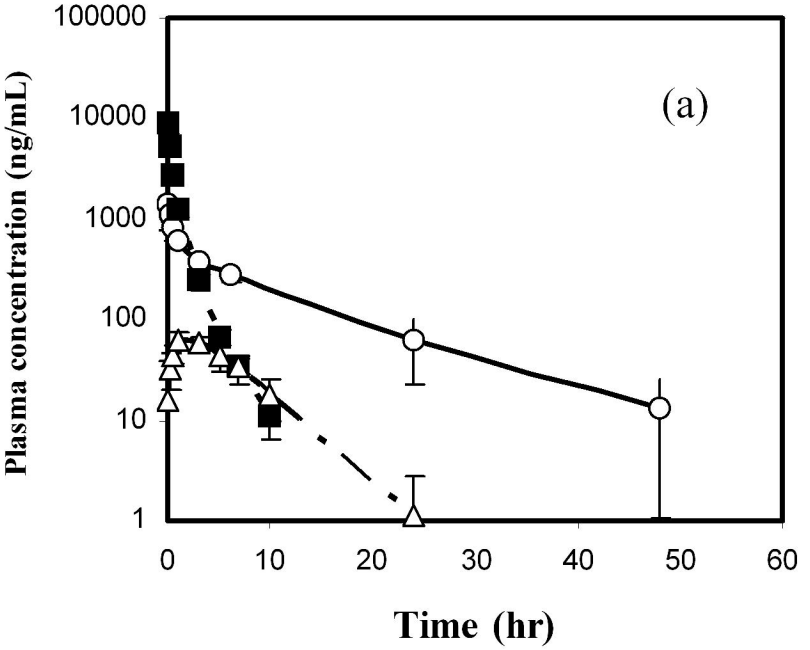
100000
10000
1000
100
10
1
Plasma concentration (ng/mL)
(a)
0
10
20
30
40
50
60
Time (hr)

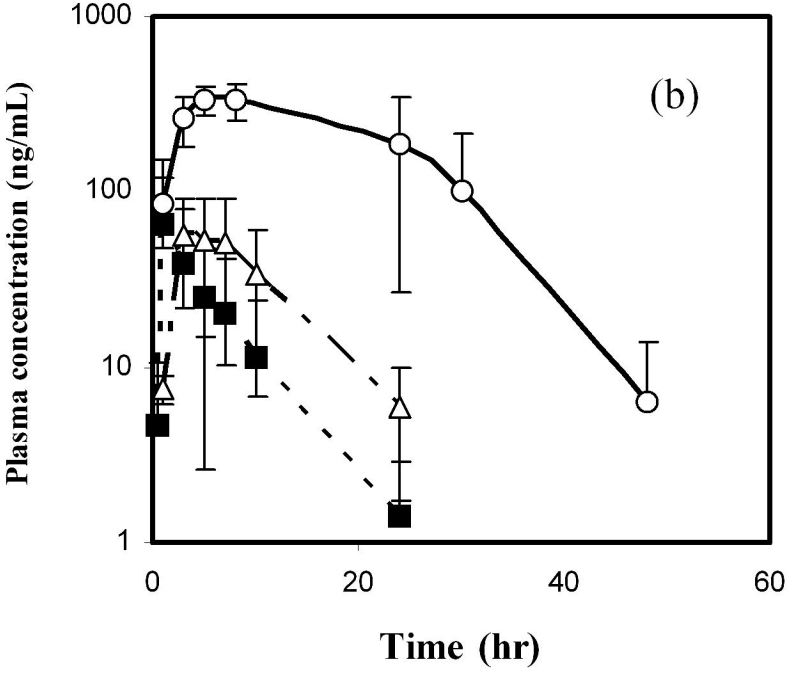
1000
100
10
1
Plasma concentration (ng/mL)
(b)
0
20
40
60
Time (hr)